# Chapter 27
# Fracture Toughness and Impact Damage Resistance of Nanoreinforced Carbon/Epoxy Composites

**Joel S. Fenner and Isaac M. Daniel**

**Abstract**  In this study, the objective was to develop, manufacture, and test hybrid nano/microcomposites with a nanoparticle reinforced matrix and demonstrate improvements to damage tolerance via Mode-II fracture toughness and impact damage absorption. The material employed was a woven carbon fiber/epoxy composite, with multi-wall carbon nanotubes as a nano-scale reinforcement to the matrix. A direct-mixing process, aided by a block copolymer dispersant and sonication, was employed to produce the nanoparticle-filled epoxy matrix. Fracture toughness was tested by several different Mode-II and mixed Mode-I/Mode-II specimens to determine the toughness improvement. Testing and material difficulties were overcome by this approach, showing a Mode-II toughness improvement of approx. 35 % in the hybrid material. Impact tests were performed in a falling-weight drop tower at different energies to introduce interlaminar damage in samples of both materials. Impact damaged specimens were imaged by ultrasonic c-scans to assess the area of the damage zone at each ply interface. Post-mortem optical microscopy confirmed the interlaminar nature of the impact damage. These tests showed a consistently smaller absorbed energy and smaller total damage area for hybrid composite over reference material, translating to a nominally higher 'effective impact toughness' in the hybrid composite (approx 42 %) regardless of specific impact energy.

**Keywords**  Nanocomposites • Hybrid nano/microcomposites • Test methods • Fracture toughness • Impact behavior

## 27.1   Introduction

The effect of nanoparticles on the mechanical properties of composite materials is an area of continuing interest in recent materials research. Such research is often motivated by the surprising enhancements that can be obtained from the introduction of relatively small quantities of nanoparticles [1–10]. The result of work in this area has considerable bearing on the possible applications of these materials and thus promotes their wider use.

Damage tolerance enhancements are to be expected from the addition of nanoparticles to a composite material owing to additional energy-absorbing mechanisms that arise. In the case of carbon nanotubes, mechanisms such as nanotube pullout from matrix, nanotube fracture, and nanotube stretching cause additional energy absorption at the nanoscale (Fig. 27.1) [2]. Mechanisms such as these contribute to bulk macroscopic energy absorption, which in turn improves overall fracture toughness and impact damage tolerance.

This objective of this study was to examine the effect of nanoparticles, namely carbon nanotubes (CNT), on the damage tolerance and energy-absorption properties of composites, especially impact damage and associated Mode-II fracture toughness, which often dominates interlaminar damage in impact [8–10].

## 27.2   Material Processing

The material employed in this investigation was a woven carbon fiber/epoxy composite with matrix reinforcement provided by short multi-wall carbon nanotubes. The major mechanical reinforcement was provided by a 5-harness satin weave carbon fabric dry preform (Hexcel, AGP370-5H, AS4 fibers, 6 k tows). The matrix was a typical Bisphenol-A epoxy resin (DGEBA, Huntsman GY 6010) cured with an anhydride hardener (Methyltetraphthalic anhydride, Huntsman HY 917)

J.S. Fenner • I.M. Daniel (✉)
Center for Intelligent Processing of Composites, Northwestern University, 2137 Tech Drive, Evanston, IL 60208, USA
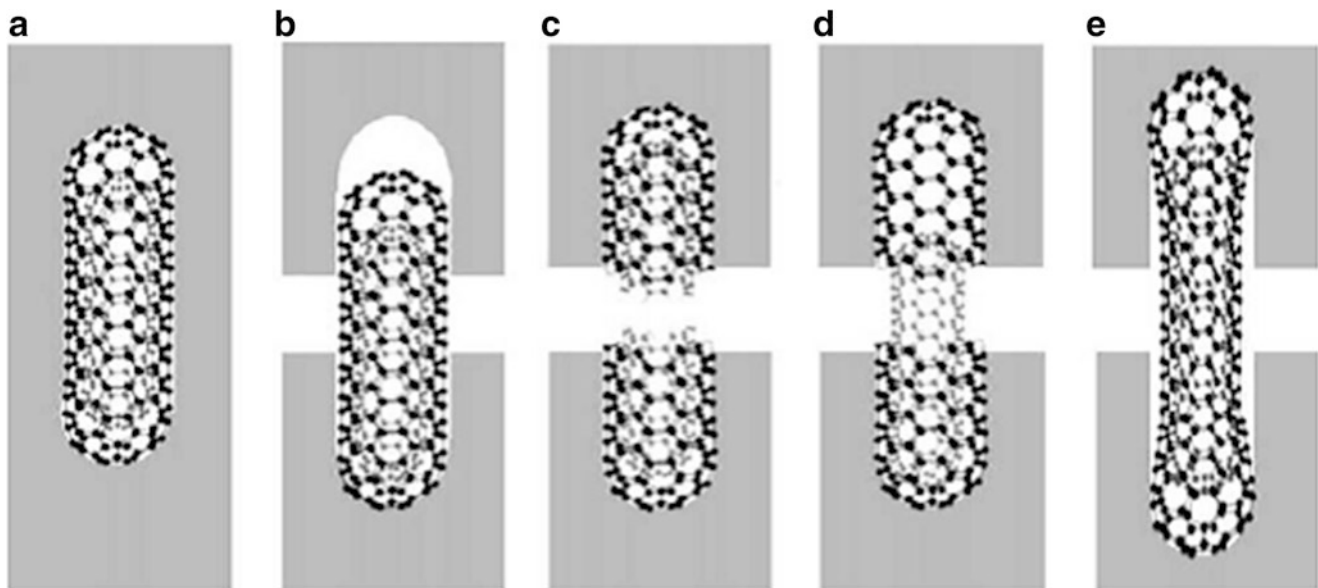e-mail: imdaniel@northwestern.edu

**Fig. 27.1** Illustration of possible energy-absorbing mechanisms of CNTs embedded in matrix: (**a**) initial state, (**b**) pullout following CNT/matrix debonding, (**c**) fracture of CNT, (**d**) telescopic pullout-fracture of outer layer and pullout of inner layer, (**e**) partial debonding and stretching [2]



1 – Composite laminate
2 – PTFE-coated release layers
3 – Lower tool plate
4 – Pressure plate
5 – Vacuum bag
6 – Resin outlet gallery
7 – Tacky-tape seal
8 – External pressure plate
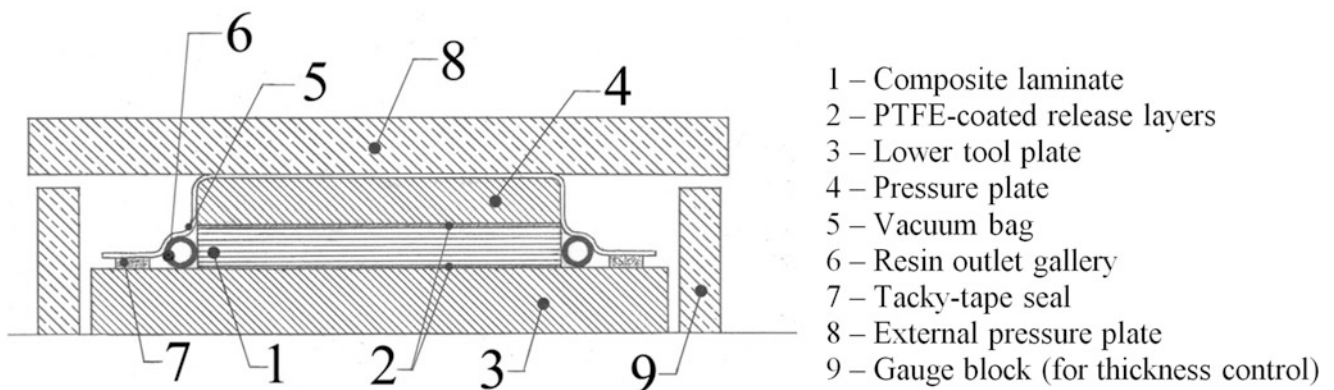9 – Gauge block (for thickness control)

**Fig. 27.2** Schematic diagram of composite fabrication mold

and an additional amine accelerator (1-Methylimidazole, Huntsman DY 070). The nominal mixture ratio was 100:90:1 (resin:hardener:accelerator) by weight. The resin was reinforced with short multi-wall carbon nanotubes (Helix Material Solutions) of 1–2 $\mu$m in length and 10–30 nm in outer diameter. A polyester block copolymer supplied in solution with a weakly volatile organic solvent (Disperbyk-2150, BYK Chemie) was used to facilitate dispersion of the CNTs [5].

Preparation of the nanoparticle enhanced matrix was carried out primarily by simple mixing and sonication. A weighed amount of DGEBA was mixed with 0.5 %wt of nanotubes and 0.5 %wt of copolymer solution. The materials were mixed together thoroughly and then vacuum degassed at an elevated temperature (80 °C) to remove the organic solvent. The anhydride hardener was then added and mixed thoroughly, followed by a repeat vacuum degassing. The resulting mixture was subjected to sonication (90 W at 20 kHz for 30 min.) to disperse the nanotubes. Just prior to composite infusion, the accelerator amine was then added, and the resin mixture infused into the carbon fiber preform, layer by layer, in a wet layup process. The wetted perform stack was subjected to final degassing and then brought to elevated temperature (150 °C) in a mold to achieve full cure. The construction of the mold (Fig. 27.2) allowed for careful control of finished laminate thickness and controlled removal of excess resin during curing. This process was developed and adapted to avoid previously encountered problems related to a marked increase in resin viscosity due to the presence of nanotubes and a filtration effect on nanotubes encountered in VARTM processing. The same procedure was used for the reference and nano-reinforced (hybrid) composites. After curing, composite plates were rough cut into specimens by means of diamond-abrasive cutting wheels, and wet-polished with SiC abrasive papers to final dimensions and smoothness.

## 27.3 Mode-II Fracture Testing

Initial Mode-II fracture toughness tests were performed by three-point End Notched Flexure (ENF), which was chosen for its overall simplicity in testing and analysis (Fig. 27.3) [11]. Specimens were prepared with nominal dimensions $L = 25$ mm, $a_0 = 7.6$ mm, $b = 12$ mm, $2h = 4$ mm (8 plies).

Tests were carried out on numerous specimens of each material type (reference & hybrid composite), giving curves of the form shown in Fig. 27.4. From these curves, calculation of the Mode-II strain energy release rate was made by various methods. For the ENF specimen, the sample compliance may be given as

$$C = \frac{\delta}{P} = \frac{1}{8bh}\left[\frac{2L^3 + 3a^3}{E_1h^2} + \frac{12L}{5G_{13}}\right] \tag{27.1}$$

where $a$ is the crack length
    $b$ is the specimen width
    $2h$ is the specimen thickness
    $E_1$ is the elastic modulus along the beam span
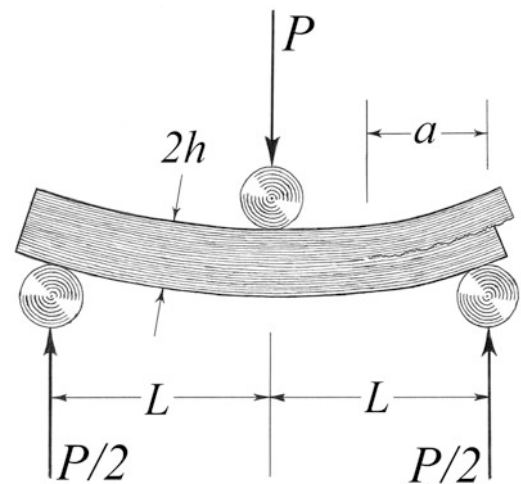    $G_{13}$ is the shear modulus in the plane of bending



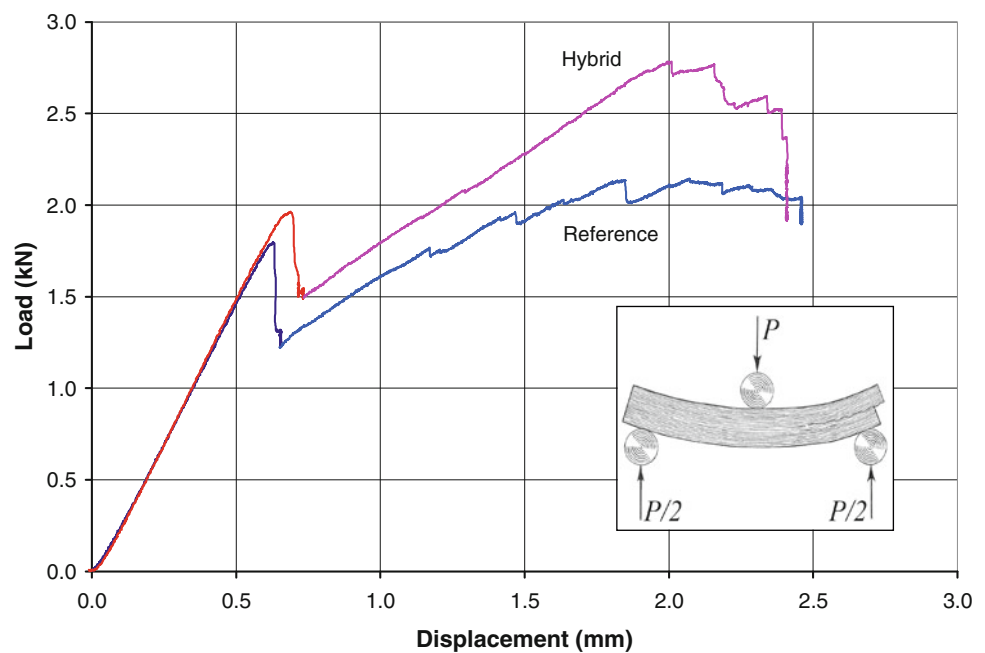**Fig. 27.3** Illustration of End Notched Flexure (ENF) test



**Fig. 27.4** Representative curves of load-displacement behavior for Mode-II ENF tests

**Table 27.1** Mode-II fracture toughness from ENF tests, calculated by various methods

| Method of calculation | Reference composite (J/m$^2$) | Hybrid composite (J/m$^2$) |
|---|---|---|
| Peak load | 553 ($\pm$200) | 729 ($\pm$239) |
| Peak load & individual specimen compliance calibration | 590 ($\pm$178) | 789 ($\pm$144) |
| Work of fracture at first release, calculated crack lengths | 1610 ($\pm$531) | 1850 ($\pm$144) |
| Work of fracture at first release, measured crack lengths | 3870 ($\pm$1340) | 3730 ($\pm$215) |

**Fig. 27.5** Theoretical behavior of a three-point end notched flexure specimen with a short ($a < a_c$) starting crack
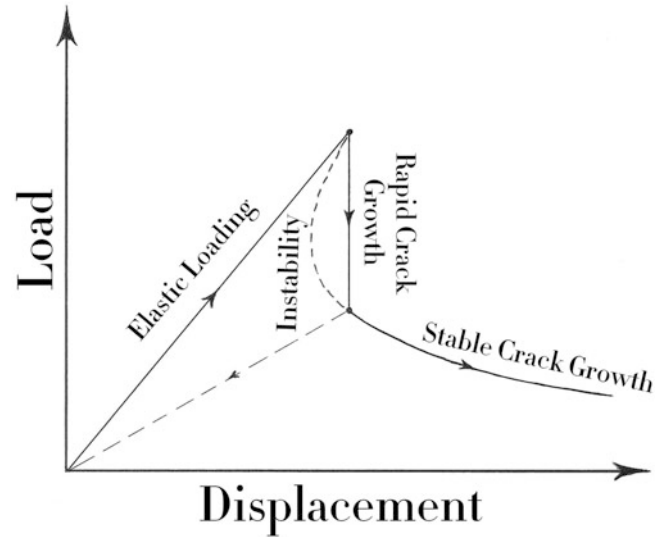


Hence, by the compliance method, the Mode-II fracture toughness at peak load at crack advance ($G_{II}$) is given by the relation

$$G_{II} = \frac{9a^2 P^2}{16E_1 b^2 h^3} \qquad (27.2)$$

where $P$ is the applied load at the central roller

Alternatively, the fracture toughness was computed making use of the loading (until first peak) and unloading (immediately after first peak) compliances of the specimen to determine the crack length. Neglecting shear effects in (27.1), the effective crack length may be calculated as

$$a \cong \left[ \frac{8\,(\delta/P)\,E_1 b h^3 - 2L^3}{3} \right]^{1/3} \qquad (27.4)$$

This permitted simple calculation of the crack length $a$ pre- and post-peak from the measured specimen compliances. Fracture toughness was then calculated by the area method as

$$G_{II} = \frac{P_1 \delta_2 - P_2 \delta_1}{2b\,(a_2 - a_1)} \qquad (27.5)$$

Calculation of the Mode-II fracture toughness purely by peak load or by peak load with initial compliance correction showed an increase of 30 % in $G_{II}$ in hybrid composite over reference composite (Table 27.1). Depending on the method of calculation, however, some disparate "apparent" values of $G_{II}$ were obtained from the data, such as those obtained using post-peak compliance or manually-measured crack lengths.

The discrepancy between various calculation methods served to indicate an obvious experimental inconsistency. In prior work on Mode-I fracture toughness with identical material [12], differing methods of calculation typically resulted in very good agreement. Furthermore, the load-displacement behavior (Fig. 27.4) of the samples did not exhibit the expected post-peak load decay that is to be expected in a typical ENF test (Fig. 27.5). These details suggested some mechanism impeding crack growth immediately after initial crack release.

**Fig. 27.6** Illustration of simple
Mode-II sliding behavior (*left*)
and Mode-II woven composite
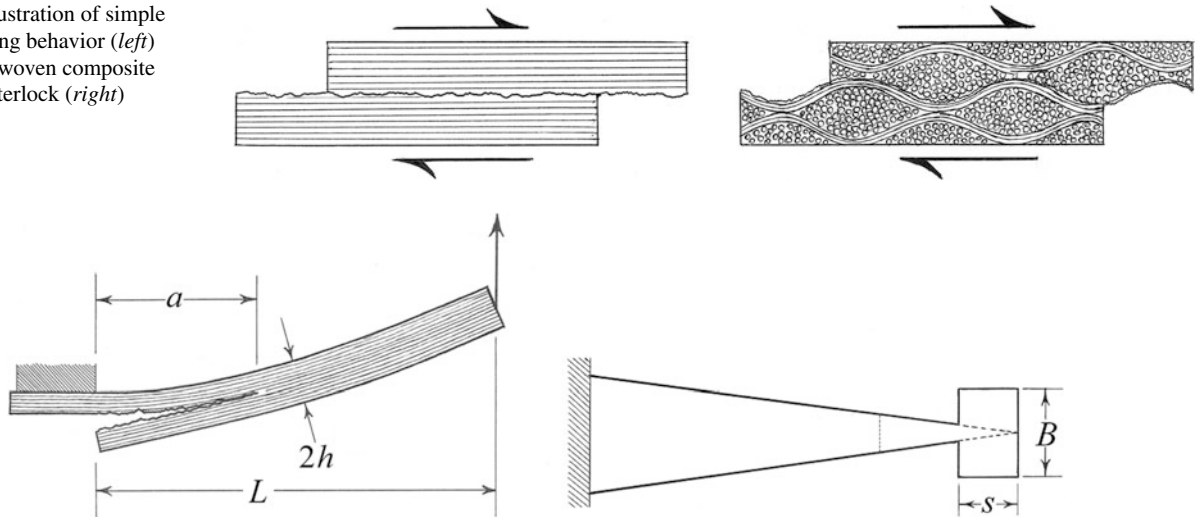ply-on-ply interlock (*right*)

**Fig. 27.7** Mixed-mode form of tapered cantilever beam specimen

The most likely cause is ply-on-ply friction or mechanical interference disturbs the outcome of this type of test, especially when employed on a woven composite material (as in Fig. 27.6) [13]. The extent of this effect is quite probably more evident in the unloading behavior rather than the loading behavior, as crack propagation involves more sliding motion than elastic loading, and as such, the values of $G_{II}$ obtained by peak loads *only* should be the most accurate. Even if this rationale is correct, there is still significant experimental variation in numerical outcome of these tests, and hence the precise values of $G_{IIc}$ for the two materials are difficult to ascertain by ENF test. The values with the highest confidence were

$G_{IIc} = 590$ ($\pm 178$) J/m$^2$ for the reference material

$G_{IIc} = 789$ ($\pm 144$) J/m$^2$ for the hybrid nano-reinforced material showing a nominal improvement of 34 % due to incorporation of carbon nanotubes.

While these tests show a marked qualitative difference between the reference and hybrid materials in Mode-II interlaminar fracture, the calculated values of Mode-II fracture toughness are unrealistically high. Most likely, this is due to a fundamental problem in testing woven composite material in pure Mode-II fracture, wherein adjacent fabric plies at an interlaminar crack plane can mechanically interfere with one another through 'interlocking' woven fiber crimps (Fig. 27.6). Because this interference impedes (or prevents) sliding of the crack faces, it causes such tests to exhibit artificially high forces at crack propagation, and hence gives artificially high values for calculated Mode-II fracture toughness. The effect also worsens with increasing crack length.

## 27.4   Mixed-Mode Testing

As a means of overcoming the difficulties encountered in pure Mode-II testing of woven composites, mixed-mode fracture tests were attempted following the general form of Fig. 27.7. In such tests, the presence of an opening-mode component alleviates interlaminar crimp-on-crimp mechanical interference by separating the crack faces.

Assuming a linear superposition of modes applies to such a specimen (Fig. 27.8) the total specimen strain energy release rate may be given as

$$G_T = \frac{21P^2k^2}{4E_1h^3} \tag{27.6}$$

where $k = a/b$ is the width taper ratio

For the complete specimen, the total fracture toughness is a merely sum of the strain energy release rates of the component modes, expressed as

**Fig. 27.8** Linear superposition components of mixed-mode cantilever beam specimen
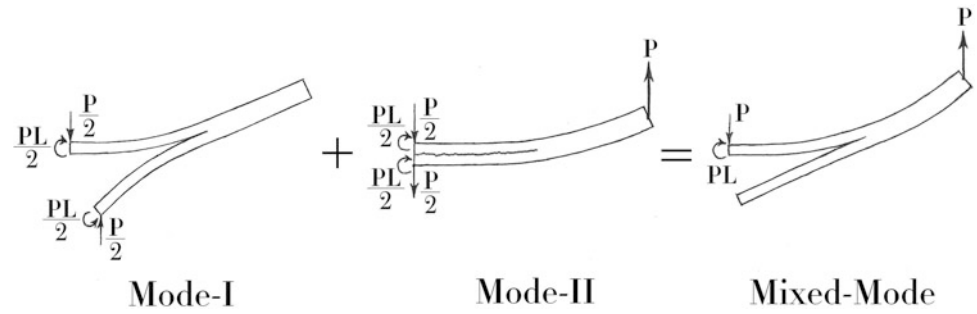


$$G_T = G_I + G_{II} \tag{27.7}$$

Thus, the fractional contributions of the different modes (I & II) in this specimen are essentially

$$\frac{G_I}{G_T} = \frac{4}{7} \tag{27.8}$$

and

$$\frac{G_{II}}{G_T} = \frac{3}{7} \tag{27.9}$$

regardless of crack length. This makes the width-tapered specimen very convenient, as it possesses constant fractional contributions from the different modes throughout a test.

However, mixed-mode testing then requires the introduction of an interaction criterion to describe the contribution of the two fracture modes (I & II) to the overall specimen load-displacement behavior at crack advance. At the present, there is no fundamentally superior theory for addressing mixed-mode fracture. For the purposes of this study, three of the most significant criteria were selected for the purpose of extracting the Mode-II component from the mixed-mode specimen response: those of Wu & Reuter [14], Benzeggagh & Kenane [15], and Reeder [16]. These criteria may be expressed as

$$\left(\frac{G_I}{G_{Ic}}\right)^{\alpha} + \left(\frac{G_{II}}{G_{IIc}}\right)^{\beta} = 1 \quad \text{Wu \& Reuter} \tag{27.10}$$

$$G_{Tc} = G_{Ic} + (G_{IIc} - G_{Ic})\left(\frac{G_{II}}{G_T}\right)^{m} \quad \text{Benzeggah \& Kenane} \tag{27.11}$$

$$G_{Tc} = G_{Ic}\left[1 - \left(\frac{G_{II}}{G_T}\right)^{m}\right] + G_{IIc}\left(\frac{G_{II}}{G_T}\right) \quad \text{Reeder} \tag{27.12}$$

All mixed-mode interaction criteria also depend on semi-empirical parameters to define the extent of interaction of the different fracture modes. Ideally, these parameters are calibrated experimentally for a given material by performing pure Mode-I and Mode-II tests followed by mixed Mode-I/Mode-II tests where the individual contributions of the different modes are known. Since the motivation for resorting to a mixed-mode attack in this case is the inability to obtain reliable values for the pure Mode-II behavior, published parameters from other studies were necessarily a resort in being able to apply these criteria. For Wu & Reuter, values of $\alpha = 1$ and $\beta = 2$ were proposed as generally valid parameters [14] for orthotropic plates. These constants were also validated experimentally by O'Brien [17], showing their applicability to carbon-fiber composite materials. For the Benzeggagh & Kenane criterion, the authors [15] suggested that a value of $m = 2$ described most brittle materials fairly well, and that a value of $m = 1.557$ fit their experimental data for a carbon/epoxy composite especially well. For the Reeder criterion, a similar value of $m = 2$ was chosen.

From prior testing by Mode-I DCB specimens [12] on identical materials, the Mode-I interlaminar fracture toughness was found to be $G_{Ic} = 176 \, (\pm 14) \, \text{J/m}^2$ for the reference material for the reference composite. This permitted calculation of the Mode-II fracture toughness by the mixed-mode criteria as (Table 27.2)

**Table 27.2** Results of calculated Mode-II fracture toughness for reference composite from mixed-mode testing by different interaction theories

|  | Wu & Reuter (J/m$^2$) | Benzeggagh-Kenane (J/m$^2$) | Reeder (J/m$^2$) |
|---|---|---|---|
| Reference composite | 475 ($\pm$255) | 556 ($\pm$90) | 312 ($\pm$56) |

**Fig. 27.9** Overview photographs of falling weight drop tower used in impact damage tests (*left*: photograph of tower and instrumentation, *right*: close view of impactor and inductive position sensor with sample in fixture prior to test)
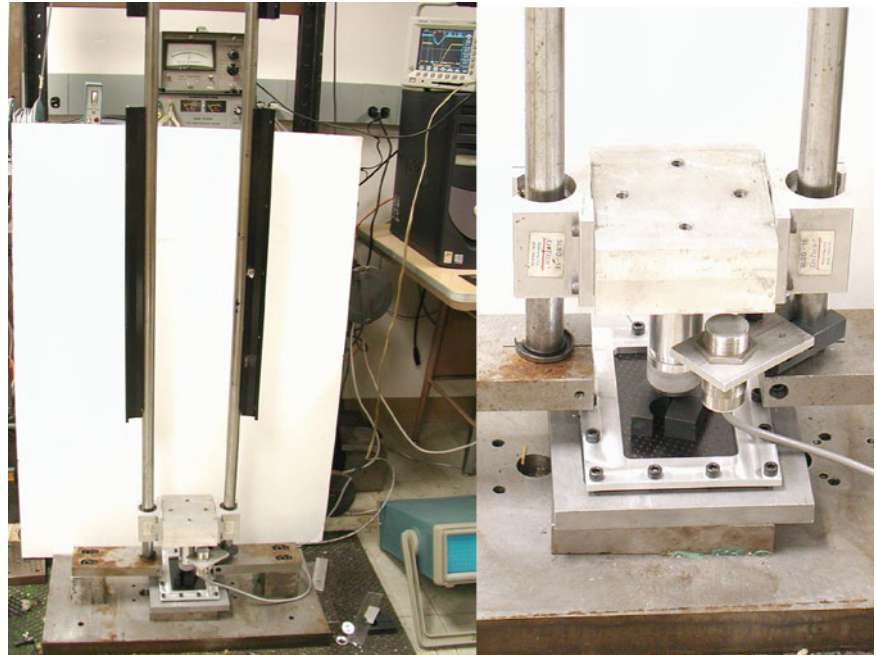


While there was some disagreement between the result obtained based on the choice of interaction criterion, all these values were somewhat close to the value of $G_{IIc} = 590$ J/m$^2$ obtained from pure Mode-II testing. The value of 556 J/m$^2$ obtained from Benzeggagh-Kenane calculations was also closest, which is perhaps due to the interaction parameter $m = 1.557$ being suggested experimentally rather than just a *generally* valid numerical parameter as in the case of the other theories. This reinforces the validity of the Mode-II fracture toughness results, which were uncertain due to testing complications.

## 27.5  Impact Testing

Impact tests were carried out in a falling-weight drop tower to introduce interlaminar damage in composite plate samples [18]. Samples were of nominal dimensions l = 150 mm (6 in), w = 100 mm (4 in), h = 5 mm (0.200 in) (16 plies), prepared by abrasive machining from larger cast plates. The drop tower was instrumented with an inductive position sensor (Fig. 27.9) to allow accurate measurement of impactor velocity immediately before and after impact, thereby allowing calculation of the absorbed impact energy as

$$E_a = \frac{1}{2} m \left( v_f^2 - v_i^2 \right) \tag{27.13}$$

where $m$ is the impactor mass

$v_i$ and $v_f$ are the pre- and post-impact velocities, respectively

From tests on multiple samples of both materials (reference and hybrid nanocomposite) at varying initial impactor heights, sufficient data were generated to produce plots of relative energy absorption as a result of impact (Fig. 27.10). These tests showed a generally lower proportion of absorbed energy in the hybrid composite. The two materials only converged at higher impact energies due to a substantial amount of obvious fiber breakage at the sample face opposite the impact site, which shows those tests to be dominated by fiber failure rather than interlaminar damage.

**Fig. 27.10** Plot of relative
energy absorption through impact
as a function of initial impactor
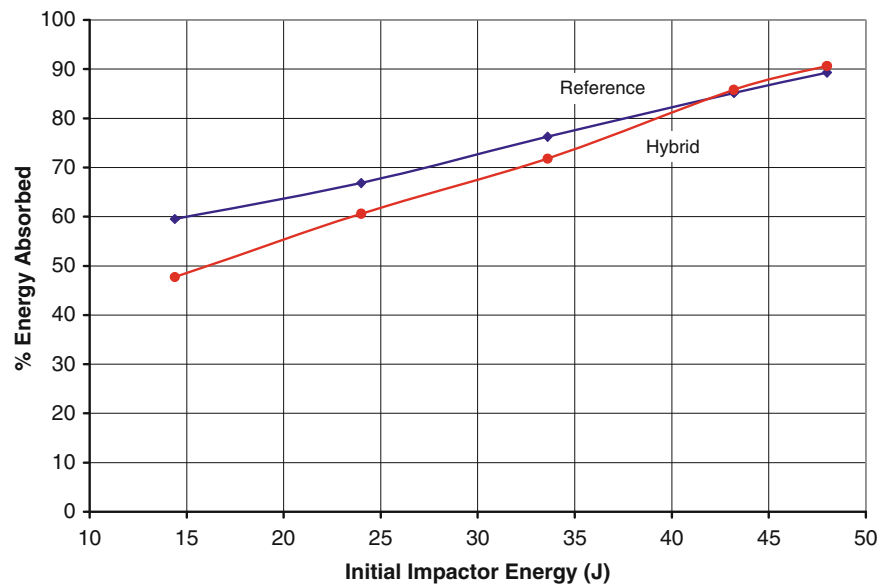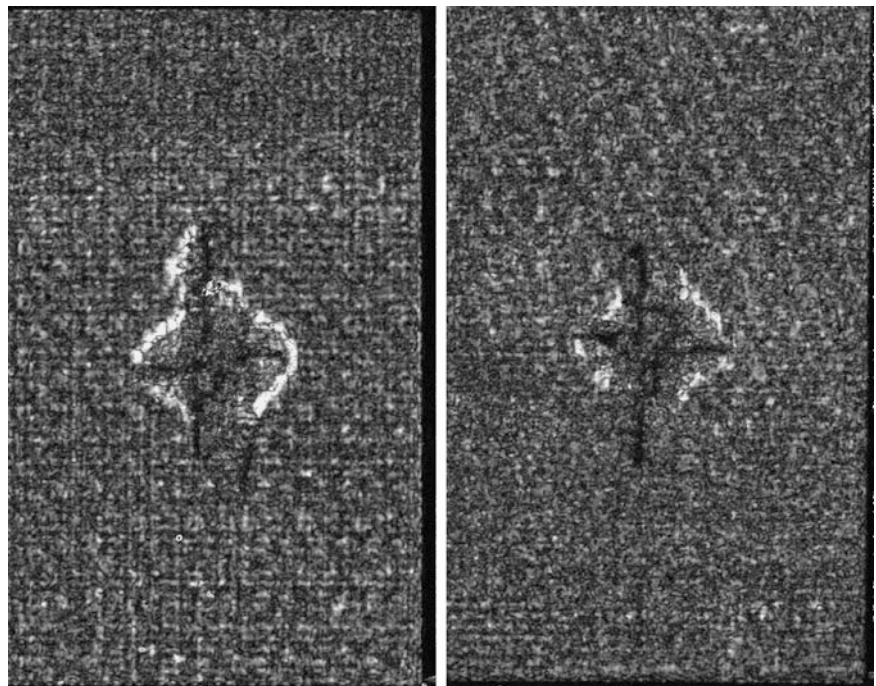potential energy for the two
materials



**Fig. 27.11** Ultrasonic C-scan
images of sample midplane
(ply 8), 40 J impact, *left*:
reference material, *right*: hybrid
material



Following impact, each sample was imaged ultrasonically in a water-immersion scanning tank utilizing a 5 MHz focused probe. Ultrasonic C-scan timing gates were specified to collect reflected wave signals separately for each of the 16 plies in the composite, permitting through-thickness imaging of the damage zone. These various C-scan images (Figs. 27.11 and 27.12) were then examined to assess the size of the damage zone at each of the 16 plies.

By digital analysis of the C-scan images (16 for each specimen tested) it was then possible to compute an individual damage are for each ply of a tested sample (Fig. 27.13), defined by the contrast boundary in the image. This in turn gave a means of quantifying the 'total damage area' for each sample, representative of the total crack surface area formed due to delamination. Computation of this quantity for each sample yielded sufficient data to produce plots showing the variation of the total damage area with absorbed impact energy (Fig. 27.14). The tests then showed a consistently smaller total damage area in the hybrid composite, again suggesting some reinforcing effect from the presence of the nanotubes.

To confirm the ultrasonic assessment of the samples, additional work was performed by cutting post-mortem cross sections and examining them by optical microscope. These studies showed undamaged material to be effectively free of interlaminar cracking (Fig. 27.15), while samples subjected to impact damage showed extensive and random cracking within the fiber

**Fig. 27.12** Ultrasonic C-scan images of sample backwall (ply 16), 40 J impact, *left*: reference material, *right*: hybrid material
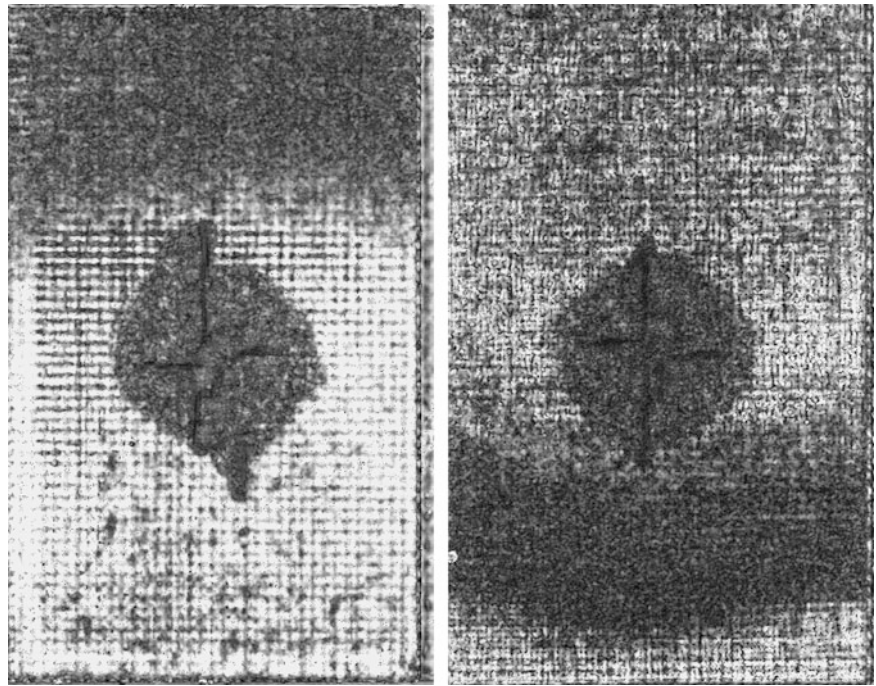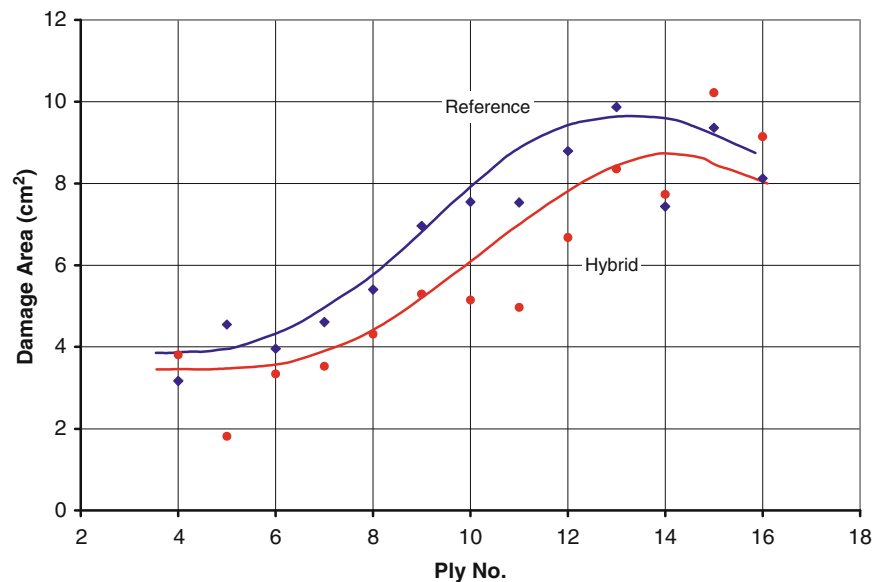


**Fig. 27.13** Representative measured damage area from ultrasonic C-scan tomographs at individual ply locations



tows of the woven material. This both confirmed the findings of ultrasonic scanning, and showed that crack formation was not merely inter-ply but also had an intra-ply component as well that was not discernable by ultrasonic imaging. As such, it implies more than one mode of fracture is present under impact conditions (Fig. 27.16).

As a means of quantifying the overall damage tolerance behavior of these materials under impact, an *effective* fracture toughness was then defined as

$$G_T \cong \frac{E_a}{A_T} \tag{27.14}$$

where $E_a$ is the absorbed impact energy for a given test

$A_T$ is the total measured delamination area (across all plies) for a given impact specimen.

While this definition possess an inherent limitation in that it does not precisely quantify *all* of the internal fracture surface produced by impact, as only the 2-D projection of that damage onto the ultrasonic C-scans is quantified, it is fairly easy to

**Fig. 27.14** Plot of measured total damage area as a function of impactor initial potential energy for the two composite materials
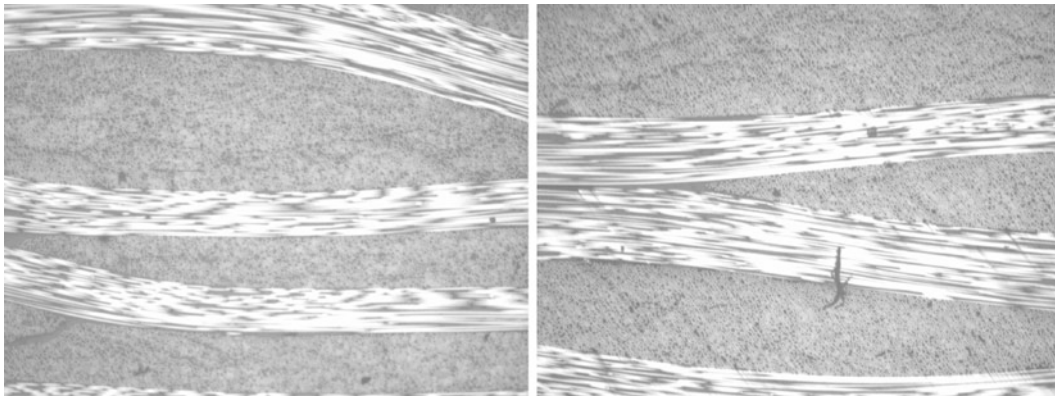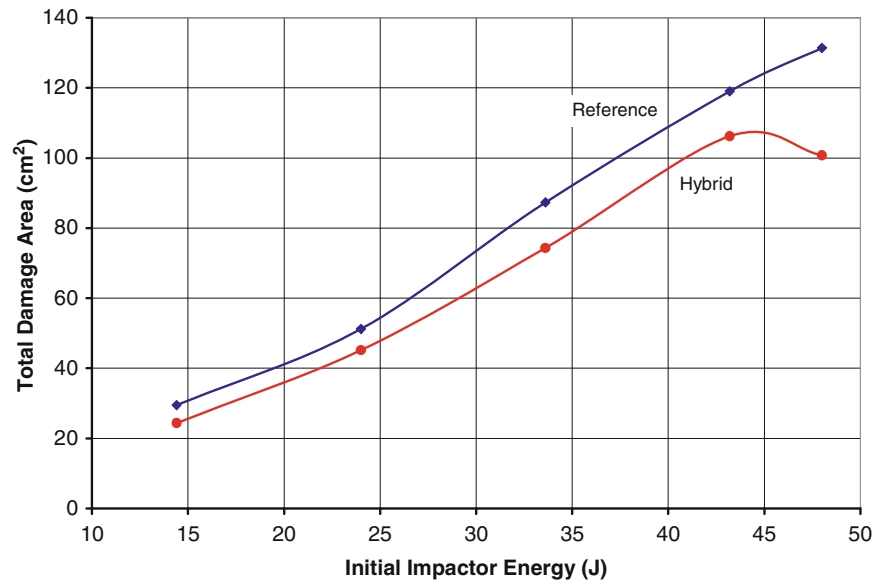


**Fig. 27.15** Optical microscope images of cut surfaces from undamaged impact testing specimens, 100× magnification (*left*: reference material, *right*: hybrid composite)
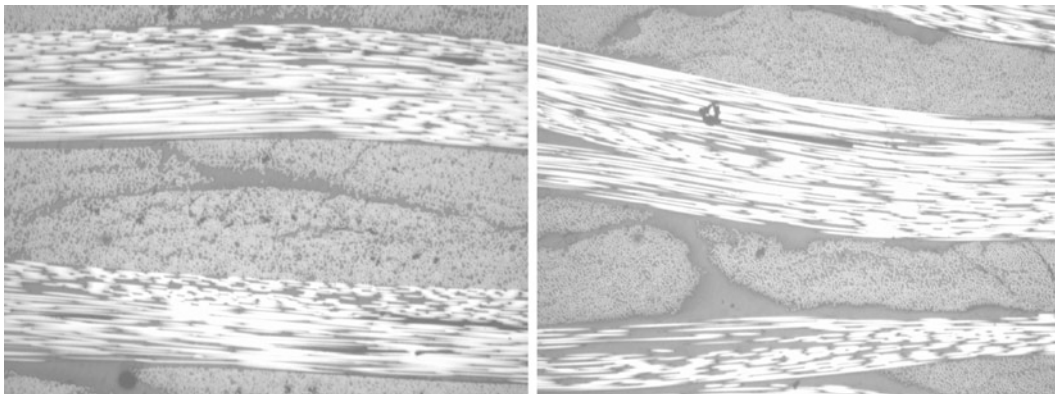


**Fig. 27.16** Optical microscope images of cut surfaces from tested impact specimens, 19 J imparted energy, 100× magnification, (*left*: reference material, *right*: hybrid composite)

calculate from the available data. By plotting absorbed impact energy as a function of total measured damage area, the slope readily gives this effective fracture toughness (Fig. 27.17)

By this method, the *effective* total fracture toughnesses were determined to be

$G_T = 3030$ J/m$^2$ for the reference material

**Fig. 27.17** Plot of absorbed impact energy as a function of total damage area showing approximate linear fits
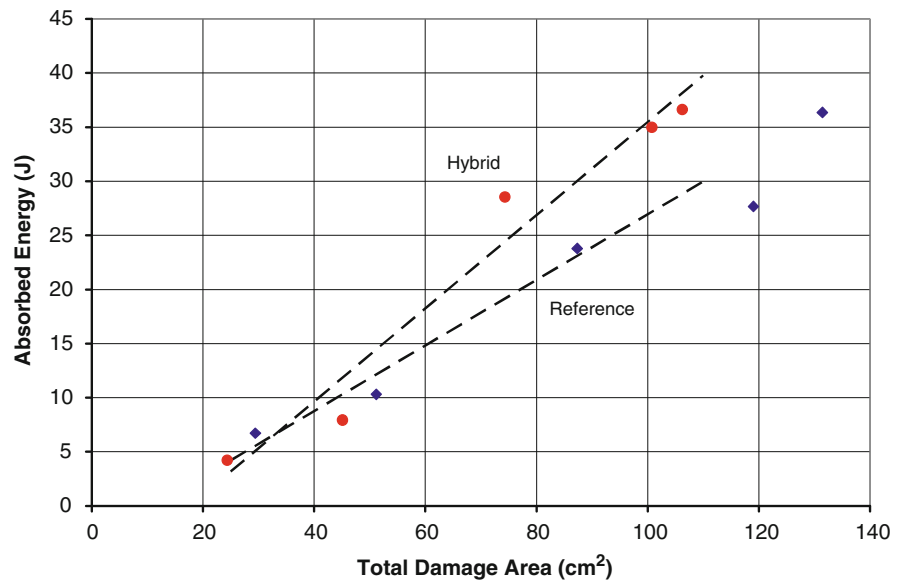


$G_T = 4300$ J/m$^2$ for the hybrid nanoreinforced material showing an improvement of 42 % due to incorporation of carbon nanotubes.

## 27.6 Conclusions

This study demonstrated that damage tolerance of fiber-reinforced composite materials can be significantly improved by nanoparticle reinforcement of the matrix at low concentrations. The presence of nanoparticles in a hybrid nano/microcomposite can offer a significant increase in interlaminar Mode-II fracture toughness, improving resistance to internal sliding delamination. Furthermore, nanoparticles also can reduce the size of internal delamination developed from impact damage to composites, reducing the overall size of an internal delamination in both diameter and through-thickness volume. In addition, the increase in Mode-II fracture toughness correlates well on a relative basis with the overall reduction in impact damage observed through the addition of carbon nanotubes to a composite.

The result of this study is significant in that it shows how overall damage tolerance of a composite, and hence its resistance to impact damage as is seen in realistic service, may be enhanced by introduction of a fairly modest quantity of nanoparticles and simple additional material processing. This not only translates to the possibility of developing more durable or robust composite materials for a broader range of applications, but also for materials that will survive significantly longer in a given application.

## References

1. Iwahori, Y., Ishiwata, S., Sumizawa, T., Ishikawa, T.: Mechanical properties improvements in two-phase and three-phase composites using carbon nano-fiber dispersed resin. Compos. A: Appl. Sci. Manuf. **36**, 1430 (2005)
2. Gojny, F.H., Malte, M.H.G., Fiedler, B., Schulte, K.: Influence of different carbon nanotubes on the mechanical properties of epoxy matrix composites-a comparative study. Comp. Sci. Technol. **65**, 2300–2313 (2005)
3. Dean, D., Obore, A.M., Richmond, S., Nyairo, E.: Multiscale fiber-reinforced nanocomposites: synthesis, processing and properties. Compos. Sci. Technol. **66**, 2135 (2006)
4. Bekyarova, E., Thostenson, E.T., Yu, A., Kim, H., Gao, J., Tang, J., Hahn, H.T., Chou, T.W., Itkis, M.E., Haddon, R.C.: Multiscale carbon nanotube-carbon fiber reinforcement for advanced epoxy composites. Langmuir **23**, 3970 (2007)
5. Cho, J.-M., Daniel, I.M.: Reinforcement of carbon/epoxy composites with MWCNTs and dispersion enhancing block copolymer. Scr. Mater. **58**, 533–536 (2008)

6. Siddiqui, N.A., Woo, R.S.C., Kim, J.K., Leung, C.C.K., Munir, A.: Mode I interlaminar fracture behavior and mechanical properties of CFRPs with nanoclay-filled epoxy matrix. Compos. A: Appl. Sci. Manuf. **38**, 449 (2007)

7. Davis, D.C., Whelan, B.D.: An experimental study of interlaminar shear fracture toughness of a nanotube reinforced composite. Compos. Part B **42**, 105–116 (2011)

8. Lin, J.C., Chang, L.C., Nien, M.H., Ho, H.L.: Mechanical behavior of various nanoparticle filled composites at low-velocity impact. Compos. Struct. **74**, 30 (2006)

9. Iqbal, K., Khan, S.U., Munir, A., Kim, J.K.: Impact damage resistance of CFRP with nanoclay-filled epoxy matrix. Comp. Sci. Technol. **69**, 1949 (2009)

10. Hosur, M.V., Chowdhury, F.H., Jeelani, S.: Processing and low-velocity impact performance of nanophased woven carbon/epoxy composite laminates. Proceedings of the Twelfth US-Japan Conference on Composite Materials, 114 (2006)

11. Carlsson, L.A., Gillespie, J.W., Pipes, J.R., Pipes, R.B.: On the analysis and design of the end notched flexure (ENF) specimen for mode II testing. J. Compos. Mater. **20**, 594 (1986)

12. Fenner, J.S., Daniel, I.M.: Hybrid nanoreinforced carbon/epoxy composites for enhanced damage tolerance and fatigue life. Compos. Part A **65**, 47 (2014)

13. Argüelles, A., Viña, J., Cantelli, A.F., Bonhomme, J.: Influence of resin type on the delamination behavior of carbon fiber reinforced composites under mode-II loading. Int. J. Damage Mech. **20**(7), 963 (2011)

14. Wu, E.M., Reuter, R.C.J.: Crack extension in fiberglass reinforced plastics and a critical examination of the general fracture criterion. Theoretical and Applied Mechanics Report No. 275 (Bureau of Naval Weapons, Contract No. NaW-64-0178-s) Urbana, (1965)

15. Kenane, M., Benzeggagh, M.L.: Measurement of mixed-mode delamination fracture toughness of unidirectional glass/epoxy composites with mixed-mode bending apparatus. Compos. Sci. Technol. **56**(4), 439 (1996)

16. Reeder, J.R.: 3D mixed mode delamination fracture criteria: an experimentalist's perspective. Proceedings of American Society for Composites, 21st Annual Technical Conference, Dearborn, (2006)

17. O'Brien, T.K.: Interlaminar fracture toughness: the long and winding road to standardization. Compos. Part B. **29**(1), 57–62 (1998)

18. ASTM Standard D7136: Standard test method for measuring the damage resistance of a fiber-reinforced polymer matrix composite to a drop-weight impact event. ASTM International: West Conshohocken (2005)